

Impulse-induced localized nonlinear modes in an electrical lattice

Faustino Palmero¹, Jesús Cuevas-Maraver², Lars Q. English³, and Ricardo Chacón⁴

¹*Grupo de Física No Lineal, Departamento de Física Aplicada I, Escuela Técnica Superior de Ingeniería Informática, Universidad de Sevilla, Avda Reina Mercedes s/n, E-41012 Sevilla, Spain*

²*Grupo de Física No Lineal, Departamento de Física Aplicada I, Escuela Politécnica Superior, Universidad de Sevilla, Virgen de África 7, 41011 Sevilla, Spain and Instituto de Matemáticas de la Universidad de Sevilla (IMUS), Edificio Celestino Mutis, Avda Reina Mercedes s/n, E-41012 Sevilla, Spain*

³*Department of Physics and Astronomy Dickinson College, Carlisle, Pennsylvania, 17013, USA and*

⁴*Departamento de Física Aplicada, E.I.I., Universidad de Extremadura, Apartado Postal 382, E-06006 Badajoz, Spain and Instituto de Computación Científica Avanzada (ICCAEx), Universidad de Extremadura, E-06006 Badajoz, Spain*

(Dated: October 16, 2021)

Intrinsic localized modes, also called discrete breathers, can exist under certain conditions in one-dimensional nonlinear electrical lattices driven by external harmonic excitations. In this work, we have studied experimentally the effectiveness of generic periodic excitations of variable waveform at generating discrete breathers in such lattices. We have found that this generation phenomenon is optimally controlled by the impulse transmitted by the external excitation (time integral over two consecutive zeros), *irrespective* of its particular waveform.

PACS numbers: 05.45.Xt, 05.45.Pq, 87.18.Bb, 74.81.Fa

I. INTRODUCTION

Intrinsic localized modes, or discrete breathers (DBs), can exist in a wide variety of coupled nonlinear oscillator networks under very general conditions [1, 2]. Specifically, they have been experimentally observed in periodically driven dissipative systems, such as Josephson junction arrays [3], coupled pendula chains [4], micro- and macro-mechanical cantilever arrays [5], granular crystals [6], and nonlinear electrical lattices [7, 8].

In all these cases, the external periodic excitations (PEs) have systematically been taken as harmonic excitations. However, there exists a vast diversity of nonlinear PEs depending upon the particular physical context under consideration. The relevance of the excitation waveform, which reflects the spectral content of the excitation's Fourier expansion, has previously been pointed out in many different backgrounds, such as ratchet transport [9], adiabatically ac driven periodic (Hamiltonian) systems [10], driven two-level systems and periodically curved waveguide arrays [11], chaotic dynamics of a pump-modulation Nd:YVO₄ laser [12], topological amplification effects in scale-free networks of signaling devices [13], and controlling chaos in starlike networks of dissipative nonlinear oscillators [14]. In all these previous works, the external T -PE $F(t)$ is chosen as a generic periodic function of zero-mean having equidistant zeros, for which it has been shown both theoretically and numerically that the *impulse* transmitted over a half period, $I = \int_0^{T/2} F(t)dt$, is the relevant quantity characterizing its clear-cut dynamical effect. It is worth noting that the relevance of the excitation impulse comes ultimately from the fact that it takes into account the *conjoint* effects of its amplitude, period, and waveform, on the one hand, and from the existence of a correlation between variations of impulse and subsequent variations of the energy transmitted by the PE, on the other hand.

Regarding DBs, it has recently been shown that the generation of stationary and moving DBs appearing in prototypical nonlinear oscillator networks subjected to non-harmonic PEs are optimally controlled by solely varying the impulse transmitted by the PEs, while keeping constant their amplitude and period [15]. Motivated by these results, we will focus in the present work on the experimental generation of stationary DBs in a nonlinear electrical lattice driven by non-harmonic PEs. We will demonstrate experimentally that this generation phenomenon is optimally controlled by the impulse transmitted by the PEs, irrespective of its particular waveform.

II. EXPERIMENTAL AND THEORETICAL SETUP

Our system, shown in Fig. 1, is a simple electrical line previously considered in Ref. [7]. Its connected nodes (circuits cells made of inductors L_2 and load resistances R) become nonlinear when including a varactor diode (NTE 618) in each of them, being the last circuit cell connected to the first one (periodic boundary conditions). The periodic driving is chosen to be spatially homogeneous; to this aim, we excite the electrical line with any previously chosen T -periodic function $V_s(t)$ by means of a programmable waveform generator. The voltage V_n at each lattice node n at point A can be readily monitorized by using oscilloscopes. In our lattice $L_1 = 0.68$ mH, $L_2 = 0.33$ mH, both with a tolerance of 10%, $R = 10$ k Ω with a tolerance of 5% and the number of nodes $N = 10$; although it may look a small number of nodes, it is large enough to get isolated one-peak DBs [7].

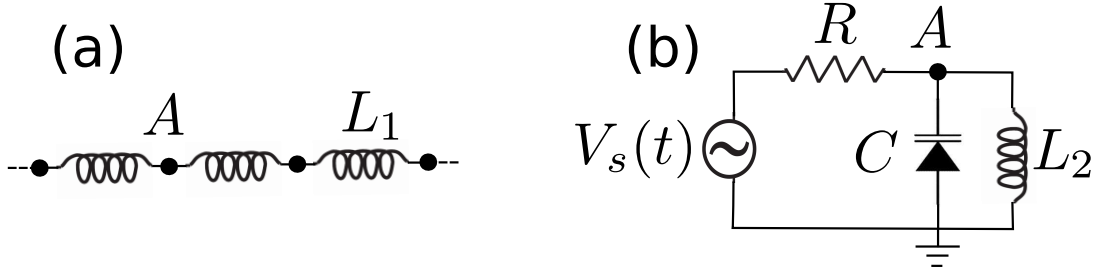


FIG. 1: Schematic circuit diagrams of the electrical transmission line (a), where the black points represent circuit cells (b). Each cell is connected to a periodic voltage source $V_s(t)$ via a resistor R , and grounded. Each point A of an elemental circuit is connected via inductors L_1 to the corresponding points A of neighboring cell. Voltages are monitored at point A .

As explicitly shown below, we will focus on the case corresponding to an external voltage source in the form $V_s(t) = A_s g(t)$, where $g(t)$ is a dimensionless and conveniently normalized T -periodic function and A_s is a voltage.

In the absence of dissipation and external PEs, an isolated circuit cell becomes a nonlinear capacitance $C(V)$ associated in parallel to an inductor L_2 , a Hamiltonian system where

$$H(p, q) = \frac{p^2}{L_2 C(q)^2} + \int_0^q x C(x) dx, \quad (1)$$

$p = L_2 C^2 \dot{V}$ and $q = V$. In the presence of the resistance R and the external PE, the variation of the energy is written as

$$\frac{dE}{dt} = L_2 C(V) \frac{dV}{dt} \left[\frac{1}{R} \frac{dV_s(t)}{dt} - \left(\frac{dI_d(V)}{dV} + \frac{1}{R} \right) \frac{dV}{dt} \right]. \quad (2)$$

Integrating over half period T (once the system has reached a steady state) and applying the first mean value theorem for integrals [13, 14], one straightforwardly obtains

$$\Delta E = - \left[\frac{1}{C} \left(\frac{1}{R} + \frac{dI_d}{dV} \right) \right]_{t=t^*} \int_{T/2} p dq + \left[\frac{p}{RC} \right]_{t=t^{**}} I, \quad (3)$$

where $t^*, t^{**} \in [0, T/2]$. According to [15], the role of the external periodic excitation $F(t)$ is played by the explicit time-dependent function $dV_s(t)/dt$, and hence $I = \int_0^{T/2} F(t) dt = V_s(T/2) - V_s(0)$ is the impulse. Note that in a more accurate model with additional dissipation sources, the impulse contribution will be unchanged.

In some cases, the basic dynamics of the electrical network composed by the aforementioned circuit cells coupled by inductors L_1 can be qualitatively described by a simple model as proposed in [7, 8], where the introduction of a phenomenological resistor in the model is enough to reproduce some experimental results. Nevertheless, in general, a more sophisticated model is necessary to match experiments. In this paper we will focus only on experimental data and the formulation of an accurate model will be object of further work.

In order to study the impulse-induced generation of stationary DBs, we conveniently chose the periodic function dV_s/dt as given in terms of Jacobian elliptic functions. Indeed, after normalizing their (natural) arguments to keep their period as a fixed independent parameter, their waveforms can be suitably changed by solely varying a single parameter: the (elliptic) shape parameter m , and hence the corresponding impulse will only depend on m once the amplitude and the period are fixed. To demonstrate that our results are independent of the particular selection of the PE, we considered two different choices:

$$\frac{dV_s^{(1)}(t)}{dt} = \frac{A_s}{T} \operatorname{sn} \left[\frac{4K(m)}{T} t; m \right], \quad (4)$$

$$\begin{aligned} \frac{dV_s^{(2)}(t)}{dt} &= \frac{A_s}{T} N(m) \operatorname{sn} \left[\frac{4K(m)}{T} t; m \right] \times \\ &\quad \operatorname{dn} \left[\frac{4K(m)}{T} t; m \right], \end{aligned} \quad (5)$$

where $N(m)$ is a normalization factor [15], $K(m)$ is the complete elliptic integral of the first kind, and $\operatorname{sn}(\cdot; m)$, $\operatorname{dn}(\cdot; m)$ are Jacobian elliptic functions of parameter m . Thus, one can change the PEs' waveform by solely varying their shape parameter

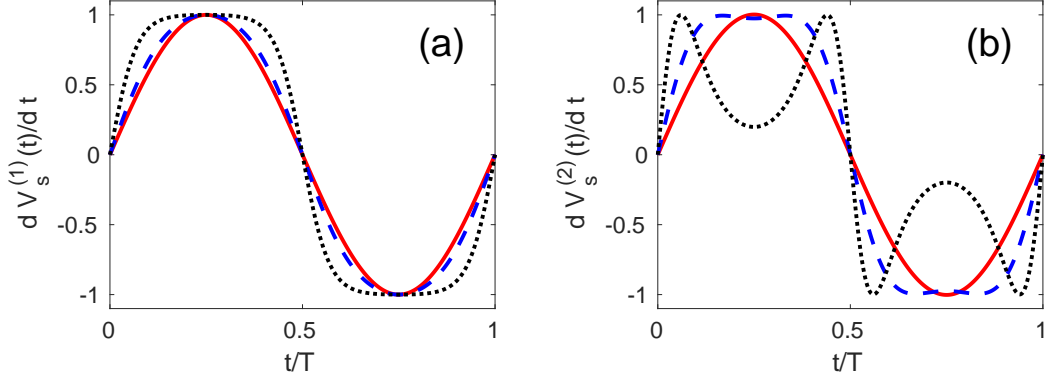


FIG. 2: (Color online) Normalized periodic excitations [given by (4) in panel (a) and by (5) in panel (b)] vs time over a period T for three values of the shape parameter: $m = 0$ (red solid line), $m = 0.6$ (blue dashed line), and $m = 0.99$ (black dotted line)

m between 0 and 1 while keeping constant their amplitude and period. If parameter m is small enough ($m \in [0, 0.8]$), a good approximation of these functions is given by the first two terms of its Fourier series which reads

$$\frac{dV_s^{(1,2)}(t)}{dt} = \frac{A_s}{T} \left[G_1^{(1,2)}(m) \sin\left(\frac{2\pi}{T}t\right) + G_3^{(1,2)}(m) \sin\left(\frac{6\pi}{T}t\right) \right], \quad (6)$$

being

$$G_1^{(1)} = \frac{2\pi}{\sqrt{m}K(m)} \frac{q^{1/2}}{1-q}, \quad (7)$$

$$G_3^{(1)} = \frac{q(1-q)}{1-q^3} G_1^{(1)}, \quad (8)$$

$$G_1^{(2)} = N(m) \frac{\pi^2}{\sqrt{m}K^2(m)} \frac{q^{1/2}}{1+q}, \quad (9)$$

$$G_3^{(2)} = \frac{3q(1+q)}{1+q^3} G_1^{(2)}, \quad (10)$$

$$(11)$$

and $q = \exp(-\pi K(1-m)/K(m))$. In Fig. 3 we depict the normalized second harmonic, $G_3(m)/G_1(m)$ as functions of the shape parameter m , for the PEs (4) and (5).

The corresponding driving functions $V_s^{(1,2)}(t)$ are written as

$$V_s^{(1)}(t) = \frac{A_s}{4\sqrt{m}K(m)} \left\{ \ln \left[\operatorname{dn} \left(\frac{4K(m)}{T}t; m \right) - \sqrt{m} \operatorname{cn} \left(\frac{4K(m)}{T}t; m \right) \right] - \ln(\sqrt{1-m}) \right\}, \quad (12)$$

$$V_s^{(2)}(t) = -\frac{A_s N(m)}{4K(m)} \operatorname{cn} \left(\frac{4K(m)}{T}t; m \right), \quad (13)$$

where $\operatorname{cn}(\cdot; m)$ is the Jacobian elliptic function of parameter m , and hence they are shift-symmetric functions: $V_s^{(1,2)}(t) = -V_s^{(1,2)}(t + T/2)$. The corresponding impulse functions read

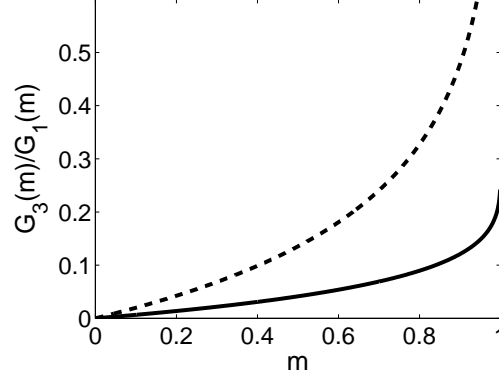


FIG. 3: (Color online) Normalized Fourier coefficients of the PEs (12) and (13) vs shape parameter m : $G_3^1(m)/G_1^1(m)$ of the PE (12) (black solid line) and $G_3^2(m)/G_1^2(m)$ of the PE (13) (black dash-dot line).

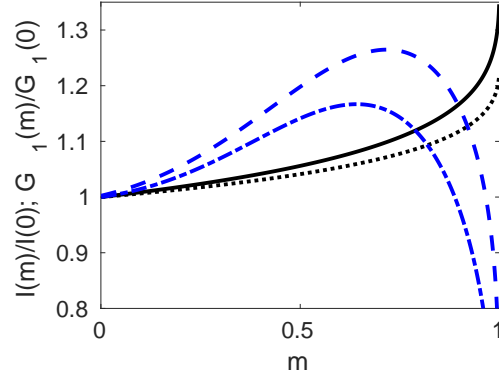


FIG. 4: (Color online) Normalized impulse functions $I^{(1,2)}(m)/I^{(1,2)}(m=0)$ and first Fourier coefficient $G_1^{(1,2)}(m)/G_1^{(1,2)}(m=0)$ as functions of the shape parameter m . Solid (black) and dashed (blue) lines correspond to the functions (14) and (15) while dotted (black) and dash-dot (blue) lines correspond to the first Fourier coefficient of (4) and (5), respectively.

$$I^{(1)}(m) = \frac{A_s}{4\sqrt{m}K(m)} \ln \left(\frac{1 + \sqrt{m}}{1 - \sqrt{m}} \right), \quad (14)$$

$$I^{(2)}(m) = \frac{A_s N(m)}{2K(m)}, \quad (15)$$

respectively. Figure 4 shows plots of the (normalized) functions $I^{(1,2)}(m)$ over the entire range $m \in [0, 1]$. It is worth noticing that these functions present different properties: While the impulse function $I^{(1)}(m)$ presents a monotonically increasing behavior for every value of m , the impulse function $I^{(2)}(m)$ presents a single maximum at $m = m_{max} \simeq 0.717$. Although the aforementioned values t^*, t^{**} will generally depend upon the shape parameter (see Eq.(3)), they become independent of the PE's waveform as $T \rightarrow 0$ [13, 14]. Note, however, that this is an unreachable limit owing to the DBs frequencies are necessarily below a certain threshold value. The first Fourier coefficient, $G_1^{(1,2)}$, of the PEs (4) and (5) is also represented in Fig. 4, featuring a qualitatively similar behaviour to that of the impulse.

III. IMPULSE-INDUCED DBS SCENARIO

Before investigating the generation of DBs in the electrical lattice, we have firstly examined in detail the response of an isolated circuit cell. Figure 5 shows the typical response of such a circuit cell, namely a nonlinear resonance curve over a certain range of values of the amplitude A_s wherein two different periodic attractors coexist, one of them exhibiting small-amplitude

oscillations whereas the other one features large-amplitude oscillations. Note that the coexistence of these two periodic attractors with clearly different amplitudes is a key ingredient for the existence of DBs [1].

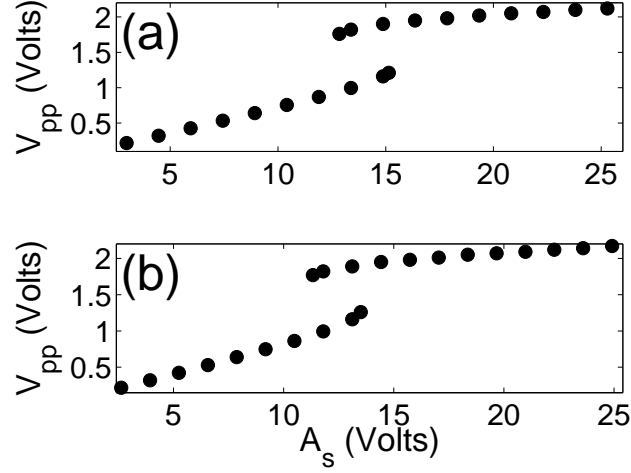


FIG. 5: (Color online) Response of an isolated circuit cell V_{pp} (peak-to-peak value of $V(t)$) as a function of the amplitude A_s for $m = 0.5$, $f = 250$ kHz, and two different driving functions $V_s(t)$, namely Eq. (12) for panel (a) and Eq. (13) for panel (b).

Figure 6 shows the critical values of the amplitude A_s giving rise to stable small-amplitude and large-amplitude periodic attractors as a function of the shape parameter m (maximum and minimum values of A_s , respectively). For the driving function (12), we have found that the threshold amplitude exhibits a monotonically decreasing behavior as a function of the shape parameter, as expected from the monotonically increasing behavior of its impulse. For the driving function (13), we found that the threshold amplitude follows the inverse behavior of its impulse such that there exists a minimum threshold at a critical value of the shape parameter: $m = m_c \approx 0.64$. Note that this critical value is relatively close to the value $m = m_{max} \approx 0.717$ at which the impulse presents a single maximum. Specifically, the critical value $m_c \approx 0.64$ corresponds to the value of m where the first harmonic of the Fourier expansion of the PE (5) presents a single maximum. In general, we have found that the threshold follows the inverse normalized first Fourier coefficients, which is in agreement with recently obtained numerical results [15] and is explicitly confirmed by our experiments (asterisks in Figs. 6 and 8).

Next, we discuss the impulse-induced generation of DBs in the full electrical line. After fixing the frequency to 250 kHz, we have found that, as expected, there exists a minimum threshold value of the amplitude A_s for which a stable one-peak localized excitation emerges, with a typical profile as in the example shown in Fig. 7. In general, as the amplitude A_s is increased, stable multi-peak breathers emerge and the DBs scenario becomes ever more complex. The ranges of amplitudes A_s wherein there exist breathers having a different number of peaks overlap with those ranges wherein there exist different families of breathers having the same number of peaks—a feature which seems to depend sensitively on the existence of small lattice impurities in our (trading) experimental components [7].

Figure 8 shows an illustrative instance of the effect of the transmitted impulse in the generation of stable DBs. We can see once again that, for the driving function (12), the threshold amplitude exhibits a monotonically decreasing behavior as a function of the shape parameter, whereas for the driving function (13) we found that the threshold amplitude follows the inverse behavior of its impulse, such that there exists a minimum threshold at a critical value of the shape parameter: $m = m_c \approx 0.64$, which is relatively close to the value $m = m_{max} \approx 0.717$ at which the impulse presents a single maximum in the aforementioned sense. Note that the first Fourier coefficient of the driving function (7) presents a single minimum at $m = m_c \approx 0.64$. The proximity of the values $m_c \approx 0.64$ and $m_{max} \approx 0.717$ can be understood from the fact that the first Fourier coefficient of the driving function (7), $G_1(m)$, already contains almost all the information of (7) regarding the effect of its impulse, which is in turn a consequence of the extremely rapid convergence of its Fourier expansion even for m values very close to 1, this being ultimately due to the dependence of $K(m)$ on m [17].

IV. CONCLUSIONS

We have experimentally investigated the effectiveness of generic periodic excitations of variable waveform at generating discrete breathers in one-dimensional nonlinear electrical lattices. Specifically, we have experimentally demonstrated for the first time that the impulse transmitted by generic periodic excitations is a fundamental quantity providing a complete control of

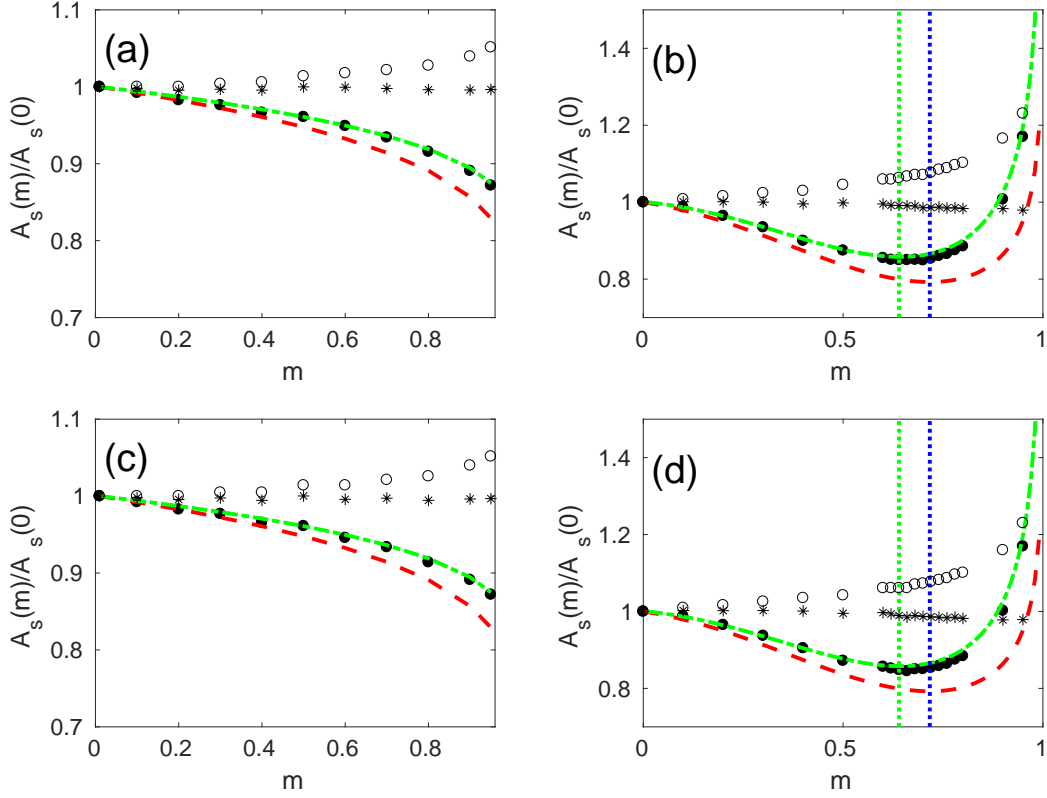


FIG. 6: (Color online) Critical values of the amplitude A_s giving rise to stable periodic attractors as a function of the shape parameter m for $f = 250$ kHz. (a, b) Maximum values of A_s for which stable small-amplitude oscillations exist. (c, d) Minimum values of A_s for which stable large-amplitude oscillations exist. Dots represent experimental data, dashed (red) lines represent the inverse of the (normalized) impulses $I^{(1,2)}(m=0)/I^{(1,2)}(m)$, dash-dot (green) lines represent the inverse of the (normalized) first Fourier coefficient $G_1^{(1,2)}(m=0)/G_1^{(1,2)}(m)$, vertical (green) dotted lines indicate the value $m \simeq 0.64$ and vertical (blue) dotted lines indicate the value $m \simeq 0.717$. Panels (a, c) correspond to the driving function (12), while panels (b, d) correspond to the driving function (13). Note that, in (b) and (d) case, close to minimum we have taken more experimental measures in order to improve the visualization of the sought phenomena. Open circles represent the experimental normalized amplitude $A_s/[I^{(1,2)}(m=0)/I^{(1,2)}(m)]$ and asterisks the corresponding experimental normalized amplitude $A_s/[G_1^{(1,2)}(m=0)/G_1^{(1,2)}(m)]$.

their effectiveness at generating discrete breathers in real-world electrical lines capable of presenting these intrinsic localized modes. We have analytically shown that this effectiveness is due to a correlation between increases in the transmitted impulse and increases in energy. Future work may extend the present impulse-induced breather-generation scenario to optimize the generation and control of diverse nonlinear localized excitations, such as kinks, solitons and vortices.

Acknowledgments

R.C. gratefully acknowledges financial support from the Ministerio de Economía y Competitividad (MINECO, Spain) through Project No. FIS2012-34902 cofinanced by FEDER funds, and from the Junta de Extremadura (JEx, Spain) through Project No. GR15146. J.C.-M. thanks financial support from MAT2016-79866-R project (AEI/FEDER, UE). Authors thank to A. Carretero-Chávez, F. Palmero-Ramos and Francisco J. Vega Narváez for their help in the experimental setup. F. P. acknowledges Dickinson College for hospitality and support.

-
- [1] S. Aubry. *Physica D* **103**, 201 (1997); S. Flach and C. R. Willis. *Phys. Rep.* **295**, 181 (1998); S. Flach and A. V. Gorbach. *Phys. Rep.* **467**, 1 (2008).
 - [2] S. Aubry. *Physica D* **216**, 1 (2006);

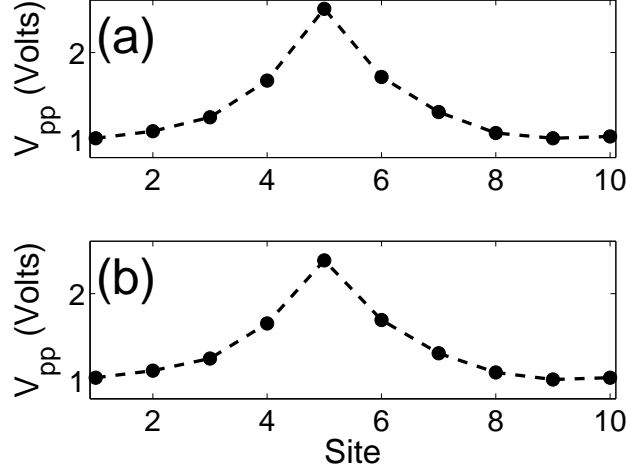


FIG. 7: Experimental (solid circles) breather profiles for $f = 250$ kHz (peak-to-peak value) and $m = 0.95$. (a) corresponds to the case (12), where $A_s = 12.4$ Volts, while (b) corresponds to the case (13), where $A_s = 16.7$ Volts. Values of A_s correspond to a threshold situation, because of smaller values of A_s implies that breather disappears.

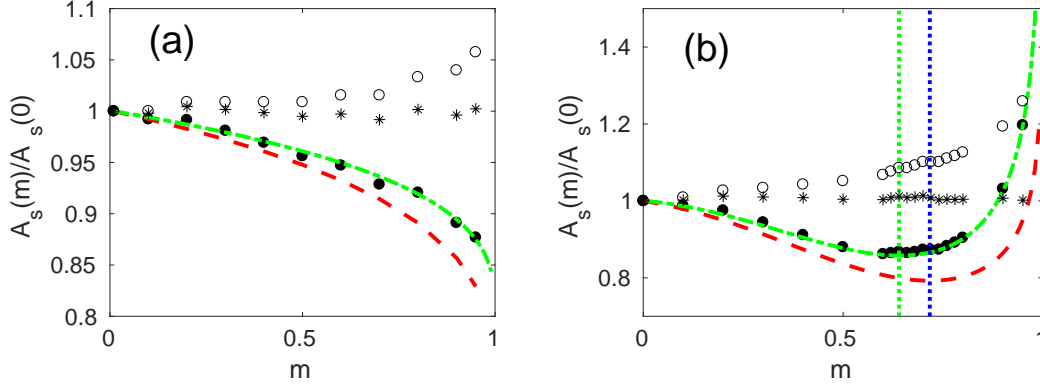


FIG. 8: (Color online) Minimum value of the amplitude A_s giving rise to the existence of a stable discrete breathers as a function of the shape parameter m for $f = 250$ kHz. Dots represent experimental values, dashed (red) lines represent the inverse of the (normalized) impulses $I^{(1,2)}(m=0)/I^{(1,2)}(m)$, dash-dot (green) lines represent the inverse of the (normalized) first Fourier coefficient $G_1^{(1,2)}(m=0)/G_1^{(1,2)}(m)$, vertical (green) dotted lines indicate the value $m \simeq 0.64$ and vertical (blue) dotted lines indicate the value $m \simeq 0.717$. Panels (a) and (b) correspond to the driving functions (12) and (13), respectively. Open circles represent the experimental normalized amplitude $A_s/[I^{(1,2)}(m=0)/I^{(1,2)}(m)]$ and asterisks the corresponding experimental normalized amplitude $A_s/[G_1^{(1,2)}(m=0)/G_1^{(1,2)}(m)]$. Note that, in panel (b), we have taken more experimental measures close to minimum for the sake of a better visualization the phenomenon.

- [3] E. Trías, J. J. Mazo and T. P. Orlando. Phys. Rev. Lett. **84**, 741 (2000). P. Binder, D. Abraimov, A. V. Ustinov, S. Flach and Y. Zolotaryuk, Phys. Rev. Lett. **84**, 745 (2000).
- [4] J. Cuevas, L. Q. English, P. G. Kevrekidis, M. Anderson, Phys. Rev. Lett. **102**, 224101 (2009); V. J. Sánchez-Morcillo, N. Jiménez, J. Chaline, A. Bouakaz, and S. Dos Santos, in Localized Excitations in Nonlinear Complex Systems (Springer International, Switzerland, 2014), pp. 251–262; J. Chaline, N. Jiménez, A. Mehrem, A. Bouakaz, S. Dos Santos and V. J. Sánchez-Morcillo. J. Ac. Soc. Am. **138**, 3600 (2015); F. Palmero, J. Han, L. Q. English, T. J. Alexander, and P. G. Kevrekidis, Phys. Lett. A **380**, 401 (2016).
- [5] M. Sato, B. E. Hubbard and A. J. Sievers. Rev. Mod. Phys. **78**, 137 (2006); M. Kimura, T. Hikihara, Chaos **19**, 013138 (2009).
- [6] N. Boechler, G. Theocharis, S. Job, P. G. Kevrekidis, M. Porter and C. Daraio. Phys. Rev. Lett. **104**, 244302 (2010); G. James, P. G. Kevrekidis, and J. Cuevas-Maraver. Physica D **251**, 39 (2013).
- [7] L. Q. English, F. Palmero, A. J. Sievers, P. G. Kevrekidis, and D. H. Barnak. Phys. Rev. E **81**, 046605 (2010); F. Palmero, L. Q. English, J. Cuevas-Maraver, R. Carretero-González and P. G. Kevrekidis. Phys. Rev. E **84**, 026605 (2011); L. Q. English, F. Palmero, P. Candiani, J. Cuevas-Maraver, R. Carretero-González, P. G. Kevrekidis and A. J. Sievers. Phys. Rev. Lett., **108**, 084101 (2012).
- [8] L. Q. English, F. Palmero, J. F. Stormes, J. Cuevas-Maraver, R. Carretero-González and P. G. Kevrekidis. Phys. Rev. E **88**, 022912 (2013).
- [9] R. Chacón, J. Phys. A **40**, F413 (2007); **43**, 322001 (2010); P. J. Martínez and R. Chacón, Phys. Rev. Lett. **100**, 144101 (2008); M. Rietmann, R. Carretero-González, and R. Chacón, Phys. Rev. A **83**, 053617 (2011).

- [10] R. Chacón, M. Yu. Uleysky, and D. V. Makarov, *Europhys. Lett.* **90**, 40003 (2010).
- [11] R. Chacón, *Phys. Rev. A* **85**, 013813 (2012).
- [12] M.-D. Wei and C.-C. Hsu, *Opt. Commun.* **285**, 1366 (2012).
- [13] P. J. Martínez and R. Chacón, *Phys. Rev. E* **93**, 042311 (2016).
- [14] R. Chacón, F. Palmero, and J. Cuevas-Maraver, *Phys. Rev. E* **93**, 062210 (2016).
- [15] J. Cuevas-Maraver, R. Chacón and F. Palmero, *Phys. Rev. E* **94**, 062206 (2016).
- [16] A.A. Qaisia and M. N. Hamdan, *J. Sound Vib.* **305**, 772 (2007).
- [17] M. Abramowitz and I. A. Stegun, *Handbook of Mathematical Functions*, Chap. 17 (Dover, New York, 1972).